Hyperfine interaction in ground and excited states of praseodymium-doped yttrium orthosilicate

J. J. Longdell,* M. J. Sellars, and N. B. Manson
Laser Physics Center, Research School of Physical Sciences and Engineering, Australian National University, Canberra, Australia
(Received 25 February 2002; published 26 June 2002)

We present characterization of the hyperfine interaction for the ground ($^3H_4$) and one optically excited state ($^1D_2$) of praseodymium impurities in a yttrium orthosilicate crystal. The Zeeman and pseudoquadrupole tensors were inferred by measuring the hyperfine splittings while rotating the direction of a weak ($\sim$40 G) magnetic field. The hyperfine spectra were recorded using Raman-heterodyne spectroscopy, a rf-optical double resonance technique.

DOI: 10.1103/PhysRevB.66.035101 PACS number(s): 61.72.−y, 31.30.Gs, 76.70.Hb

I. INTRODUCTION

Praseodymium doped Y_2SiO_5 has received increased attention of late because of its use in the demonstration of solid state optical EIT (electromagnetically induced transparency),[1] as well as its use in quantum computing proposals[2] and its use in slow light and light storage experiments.[3] It was chosen for such experiments because of its small inhomogeneous broadening in the ground state hyperfine levels, its long coherence times and adequate oscillator strengths.

Current EIT experiments using this material[1,3] have been performed in zero magnetic field due to the absence of full knowledge of the hyperfine structure. Working with nonzero magnetic fields provides a promising way to improve the limiting parameters in such experiments. For small fields the inhomogeneous broadening for the $+x/2 \leftrightarrow -x/2$ spin transition will be much less than for $\pm x/2 \leftrightarrow \pm y/2$, allowing narrower EIT features. The homogeneous linewidth for the spin transition can also be significantly reduced by applying a magnetic field.[4] This work provides the required information on oscillator strengths and transition frequencies as a function of magnetic field for the design of further EIT experiments.

Yttrium orthosilicate has symmetry given by the C_{2h}^6 space group with four formula units of Y_2SiO_5 per translational unit. This gives eight different sites at which the praseodymium can substitute yttrium. The four sites can be divided into two groups of four with the members of each pair related to each other by the crystals C_2 axis and inversion.

The pairs have different crystal field splittings. Here we are only concerned with ''site 1,'' for which the optical transition between the lowest energy components of the $^3H_4$ and $^1D_2$ multiplets is at 605.7 nm. The sites have C_1 symmetry. While in many applications this is useful in that the low symmetry relaxes selection rules in the hyperfine manifolds, it does make interpreting the spectra more difficult as there are no symmetry conditions. The crystal on which the measurements were performed consists of 0.05% praseodymium which has only one naturally occurring isotope (Pr^{141}, $I=5/2$).

II. THE THEORY OF HYPERFINE INTERACTIONS

The following Hamiltonian describes the Praseodymium nucleus and *f* electrons:

$$H=\{H_{\mathrm{FI}}+H_{\mathrm{CF}}\}+\{H_{\mathrm{HF}}+H_Q+H_z+H_{\mathrm{Z}}\}. \tag{1}$$

The six terms on the right represent the free ion, crystal field, hyperfine, nuclear quadrupole, electronic Zeeman, and nuclear Zeeman Hamiltonians, respectively. The first group of terms are much larger than the second and are what determine the electronic energy levels. The perturbation caused by the second group of terms gives the electronic levels hyperfine structure.

In the case of $Pr:Y_2SiO_5$ the $L-S$ coupling present in H_{FI} breaks the degeneracy of the $4f^2$ configuration. The crystal field (H_{CF}) breaks the degeneracy of these multiplets, and because of the low symmetry of the crystal field each member of the multiplets is an orbital singlet. Due to this ''quenching'' of angular momentum there is no first order perturbation resulting from the second group of terms of Eq. (1). The hyperfine and magnetic effects appear at the level of second order perturbations. We are interested in the transitions between the lowest members of these multiplets. Applying this second order perturbation gives for a particular hyperfine manifold the following effective spin Hamiltonian:[5]

$$H=\boldsymbol{B}\cdot(g_J^2\mu_B^2\boldsymbol{\Lambda})\cdot\boldsymbol{B}+\boldsymbol{B}\cdot(\gamma_N\mathbf{E}+2A_Jg_J\mu_B\boldsymbol{\Lambda})\cdot\boldsymbol{I} \tag{2}$$

$$+\boldsymbol{I}\cdot(A_J^2\boldsymbol{\Lambda}+\boldsymbol{T}_{\mathrm{Q}})\cdot\boldsymbol{I}. \tag{3}$$

The tensor $\boldsymbol{\Lambda}$ is given by

$$\Lambda_{\alpha\beta}=\sum_{n=1}^{2J+1}\frac{\langle 0|J_\alpha|n\rangle\langle n|J_\beta|0\rangle}{\Delta E_{n,0}}. \tag{4}$$

$\boldsymbol{E}$ is the 3×3 identity matrix, $\boldsymbol{B}$ is the magnetic field, and $\boldsymbol{I}$ is the vector of nuclear spin operators, g_J is the Lande g value, γ_N is the nuclear gyromagnetic ratio, and A_J is the hyperfine interaction parameter. The term $\boldsymbol{I}\cdot\boldsymbol{T}_{\mathrm{Q}}\cdot\boldsymbol{I}$ describes the nuclear electric quadrupole interaction. The term $A_J^2\boldsymbol{I}\cdot\boldsymbol{\Lambda}\cdot\boldsymbol{I}$ which has the same form as $\boldsymbol{I}\cdot\boldsymbol{T}_{\mathrm{Q}}\cdot\boldsymbol{I}$ is due to the second order magnetic hyperfine, also known as the pseudoquadrupole interaction.[6]

For this work the first term in Eq. (2) was neglected, as it makes no changes to the hyperfine splittings and has a small effect on the optical frequency for the small magnetic field values used. Hence the Hamiltonian used to fit the data can be written as

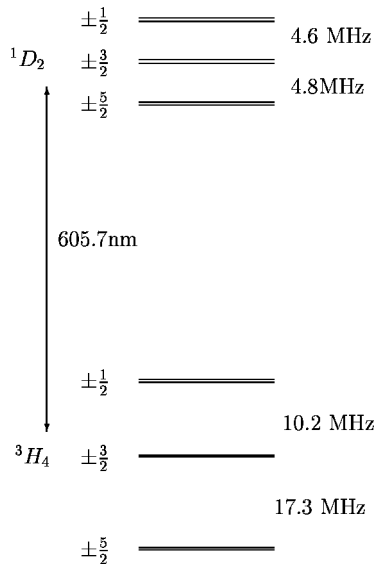

FIG. 1. Zero field energy level diagram for $Pr:Y_2SiO_5$.

$$H = \boldsymbol{B}\cdot\boldsymbol{M}\cdot\boldsymbol{I} + \boldsymbol{I}\cdot\boldsymbol{Q}\cdot\boldsymbol{I}. \tag{5}$$

The zero field energy level diagram for $Pr:Y_2SiO_5$ in ''Site 1'' is shown in Fig. 1. Each of the six membered hyperfine manifolds are split into three degenerate pairs by the term $\boldsymbol{I}\cdot\boldsymbol{Q}\cdot\boldsymbol{I}$. At zero magnetic field Raman heterodyne signals can be seen at 10.2, 17.3, 4.6, 4.8 MHz. The application of a magnetic field splits the degenerate pairs and for a 40 G magnetic the splitting is of order 1 MHz. For each orientation of ''site 1'' in the crystal, each of the above Raman heterodyne lines splits into four. The line splits into eight in general because of the two possible orientations of ''site 1.''

The inhomogeneous broadening in the hyperfine levels comes from the inhomogeneous broadening in the Λ tensor of Eq. 2. It can be seen that for small fields the inhomogeneous broadening in the Zeeman term will be small. This could allow narrower EIT to be observed using the $\pm x/2$ hyperfine levels as ground states.

III. EXPERIMENT

The crystal was cooled to liquid helium temperatures and mounted in a set of small superconducting X, Y, and Z coils which which enabled a field of ~ 40 G to be generated in any direction. To take Raman-heterodyne spectra[7,8] light from a frequency stabilized dye laser (1 MHz) was incident on the sample. The frequency of the light was tuned to be resonant with the transition from the lowest level to the lowest level of the $^3H_4$ and $^1D_2$ multiplets. A swept radio-frequency (rf) field was applied to the sample using an six-turn coil wrapped around the sample. When the rf field is resonant with a hyperfine transition a coherence is produced between the hyperfine levels. This coherence, along with that induced by the laser, creates another optical field with the same mode characteristics as the laser and a frequency shifted by the rf frequency (see Fig. 2). This created optical field is detected as a beat on the transmitted light. The signal was averaged on a digital oscilloscope and stored on a PC.

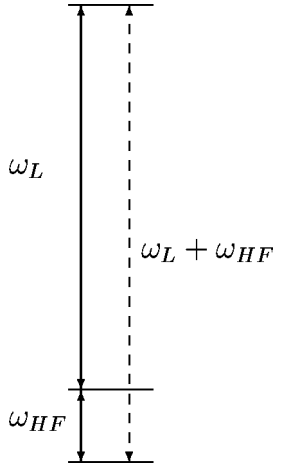

FIG. 2. Energy levels involved in the Raman Heterodyne detection. The applied optical and RF fields are ω_L and $\omega_H F$, respectively. The produced Raman field $\omega_L + \omega_H F$ gives a beat with the transmitted ω_L.

With a computer controlled current supply this enabled automated collection of the data.

For the ground state the the spectra were recorded as the magnetic field was rotated in a spiral of the form

$$\boldsymbol{B} = \begin{bmatrix} B_0\sqrt{1-t^2}\cos 6\pi t \\ B_0\sqrt{1-t^2}\sin 6\pi t \\ B_0 t \end{bmatrix}, \quad t \in [-1,1]. \tag{6}$$

The experimental data for the ground state is shown in Fig. 3 and the magnetic field values used are plotted in Fig. 4. For the excited state the magnetic field was rotated in cones about each axis, as it was desirable to have larger fields for the excited state to help resolve all the lines present. This was most easily achieved by having a larger noncomputer-controlled current supply one of the three channels. The experimental data for the excited state is shown in Fig. 5 with the magnetic field values used plotted in Fig. 6.

IV. FITTING PROCEDURE

Along with the orientation of the principal axes two parameters are required to determine the pseudoquadrupole tensors. For this work the following parametrization was used:

$$\boldsymbol{Q} = R(\alpha,\beta,\gamma)\begin{bmatrix} -E & 0 & 0 \\ 0 & E & 0 \\ 0 & 0 & D \end{bmatrix} R^T(\alpha,\beta,\gamma), \tag{7}$$

where $R(\alpha,\beta,\gamma)$ is the rotation matrix defined by the three Euler angles (α,β,γ).[9] For the Zeeman tensor there are six independent parameters and the following parametrization was used:

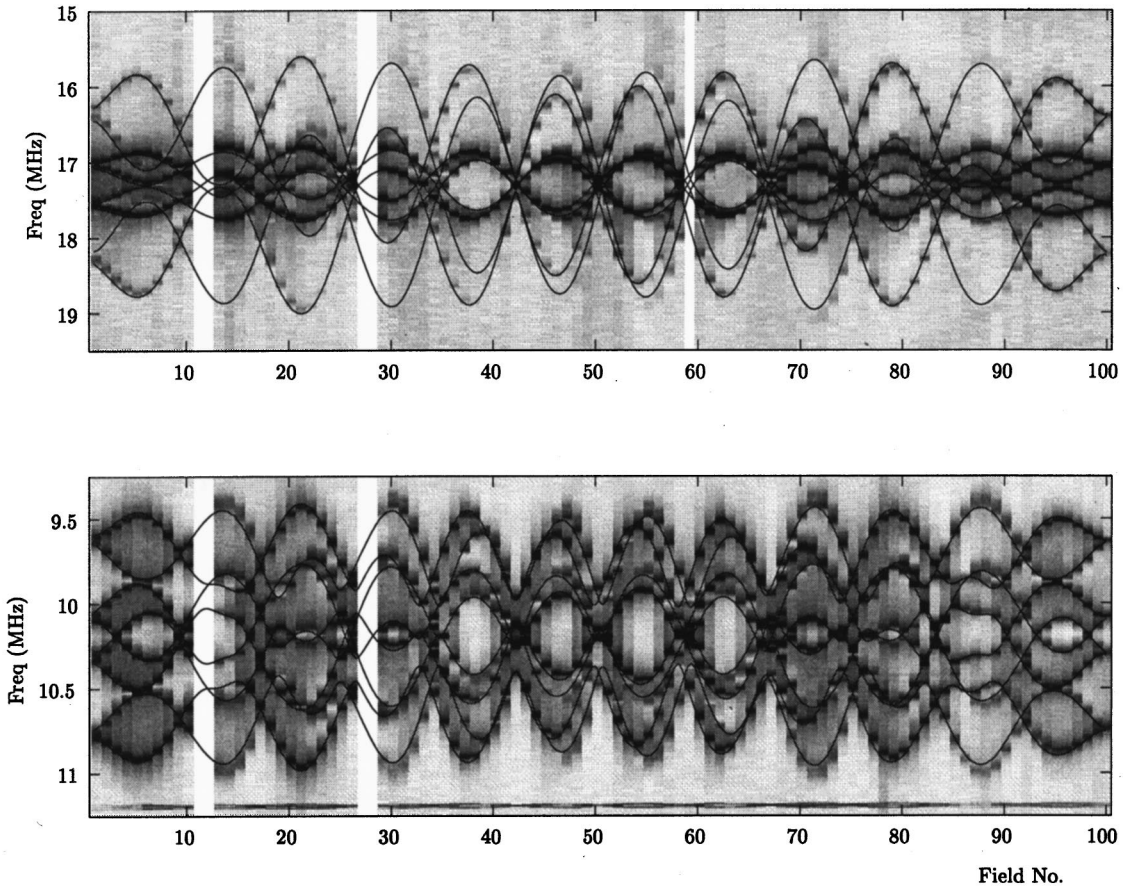

FIG. 3. The hyperfine spectra obtained for the ground state. Each vertical slice is one spectra with darkness indicating intensity of Raman heterodyne signal. The field was varied along the horizontal axis as described in the text.

$$\boldsymbol{M}=R(\alpha,\beta,\gamma)\begin{bmatrix} g_x & 0 & 0 \\ 0 & g_y & 0 \\ 0 & 0 & g_z \end{bmatrix} R^T(\alpha,\beta,\gamma). \tag{8}$$

In the case of system with no true quadrupole interaction it can be easily seen from Eq. (2) that the principle axes of the two tensors $\boldsymbol{M}$ and $\boldsymbol{Q}$ will be aligned. Further to this as the parameter apart from $\boldsymbol{\Lambda}$ are known there are only three parameters in addition to the orientation of the tensors which are independent. The absolute values of the parameters D and E can be determined from zero-field quadrupole splittings; however, their signs cannot. Three different models were used to try and fit the data: one where it was assumed that there was no real quadrupole interaction, one where the tensors $\boldsymbol{M}$ and $\boldsymbol{Q}$ were taken to share the same axes but the principle values were allowed to vary freely, and one where no relationship was assumed between the two tensors.

The position of the C_2 axis was nominally along the y axis but was included as a parameter because of the small misalignment between the coils and the sample. There is uncertainty in the parameters D and E obtained at zero field and hence their value is allowed to vary on fitting the data. This uncertainty arises from a small background field giving the lines an extra broadening at zero applied field.

The positions of all the peaks were determined manually from the recorded spectra. This data was then fed into a computer program that minimized the difference between the experimental values and those expected from a pair of systems, one with a Hamiltonian

$$H=\boldsymbol{B}\cdot\boldsymbol{M}_1\cdot\boldsymbol{I}+\boldsymbol{I}\cdot\boldsymbol{Q}_1\cdot\boldsymbol{I} \tag{9}$$

and the other with a Hamiltonian

$$H=\boldsymbol{B}\cdot\boldsymbol{M}_2\cdot\boldsymbol{I}+\boldsymbol{I}\cdot\boldsymbol{Q}_2\cdot\boldsymbol{I}. \tag{10}$$

Here each $\boldsymbol{X}_1$ and $\boldsymbol{X}_2$ are related to each other via the C_2 axis. The tensors $\boldsymbol{M}_1$, $\boldsymbol{Q}_1$, and the position of the C_2 axes were the varied parameters.

The minimization was carried out using a simulated annealing[10] method. When implementing such an algorithm there is freedom in choosing two characteristics, how you lower the ''temperature'' and how you choose the proposed state. In order to find the solution which minimized the error, the initial temperature was chosen at a level corresponding to a uncertainty in the spectral lines of about 1 MHz. It was then lowered exponentially to 1 kHz over two million jumps, at which point it was no longer changing. This was repeated a few times with different initial conditions and random number seeds to confirm that the true minimum had been found. For the evolution step one of the system parameters

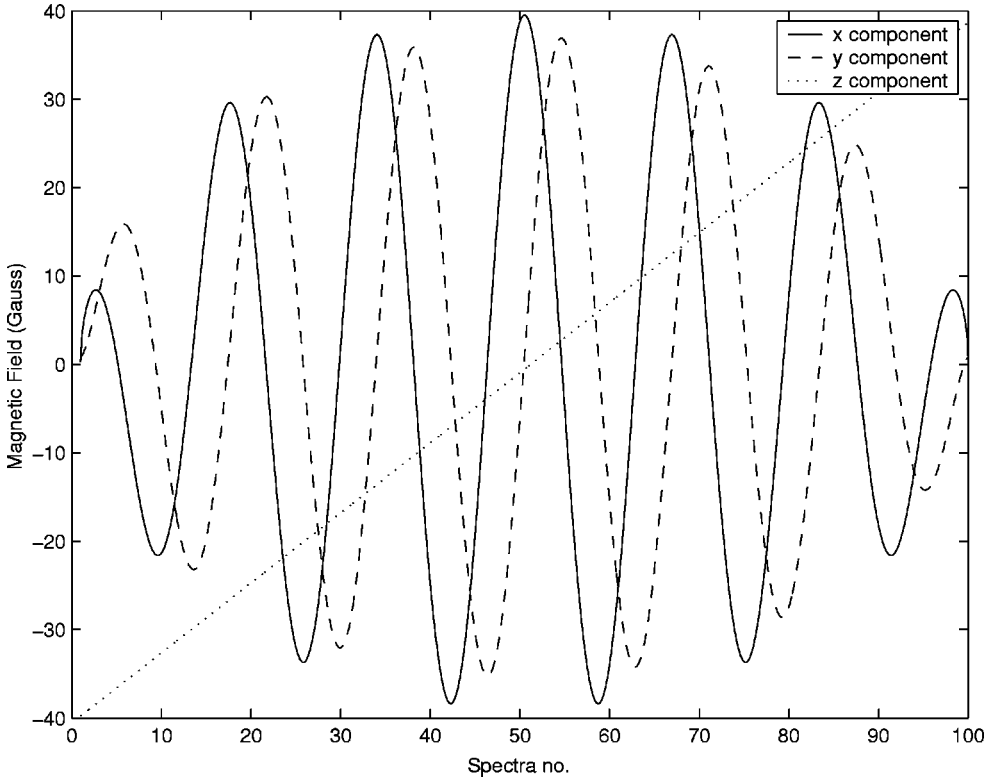

FIG. 4. Magnetic field values used to obtain ground state hyperfine spectra.

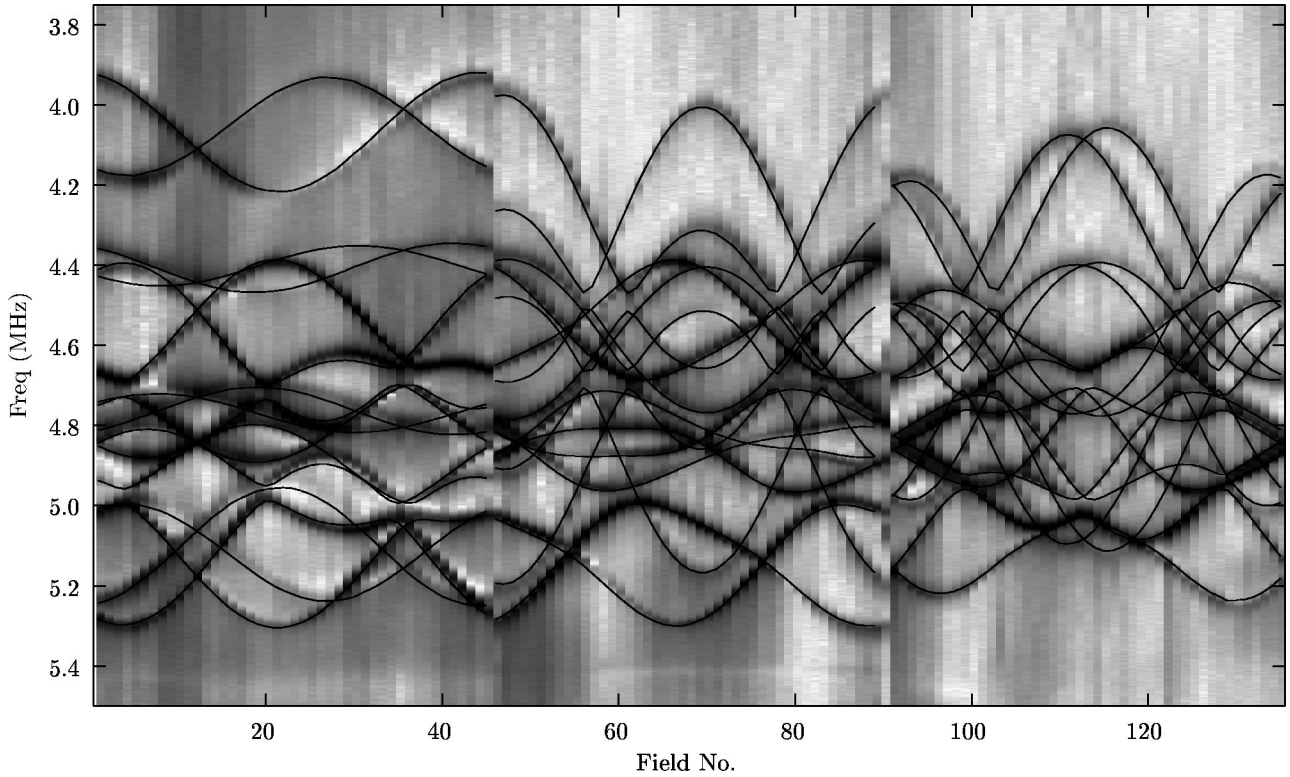

FIG. 5. The hyperfine spectra obtained for the optically excited state. Each vertical slice is one spectra with darkness indicating intensity of Raman heterodyne signal. The field was varied along the horizontal axis as described in the text.

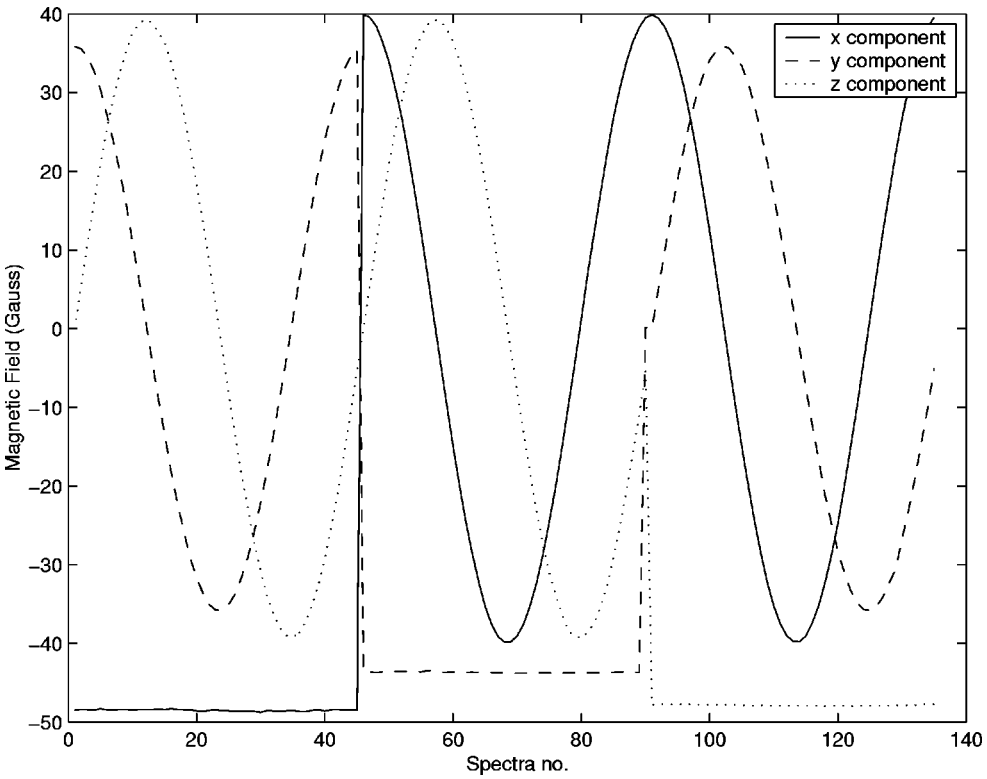

FIG. 6. Magnetic field values used to obtain excited state hyperfine spectra.

was chosen at random and a random variable with a Lorentzian distribution was added to it. The initial width (it has infinite variance) of this distribution was chose to be about five degrees for angles and 10% of the expected results for other quantities. These were also reduced exponentially but at a rate three times slower than the temperature.

V. RESULTS

The spectra along with the best theoretical fit are shown in Figs. 3 and 5. The r.m.s. deviation between the measured and fitted lines is 23 kHz for the ground state and 7 kHz for the excited state. Uncertainties in the determined parameters were found by reducing the ''temperature'' to a value above zero in the annealing algorithm. Such a method can be shown to be rigorous if all the uncertainty was due to Gaussian noise in the peak positions. In this situation, however, various systematic errors were also important.

The ''final temperature'' was chosen to correspond to a standard deviation of 30 kHz in the peak positions, roughly equal to the linewidths of the hyperfine spectra. The results are shown in Tables I and II. The random errors are due to the uncertainty in the fit while the total error includes various systematic errors. These include the measurement of the frequency, background magnetic fields, and imperfections in the xyz coils but do not include uncertainty due to misalignment of the crystal. This misalignment is the greatest source of uncertainty in the determined values and is of the order of $5°$.

The position of the C_2 axes were in both cases close to the y axis. The difference between the position of the C_2 axis and the y axis represents how well the crystal was aligned in the xyz coils. It should be noted that the crystal was taken out and remounted between the collection of the ground and excited state data.

For the ground state the difference between the principle axes of the Zeeman and pseudoquadrupole tensors was resolved, but the difference was small ($<5°$). This would be expected if the pseudoquadrupole was much greater than the real quadrupole interaction, however, the data could not be well explained by a model where the real quadrupole contribution was neglected. In the excited state the Zeeman and pseudo quadrupole tensors are not aligned, however, the

TABLE I. Results for fitting of the ground state.

Quantity	Value	Random uncertainty	Total uncertainty	Units
E	0.5624	0.0002	0.003	MHz
D	4.4450	0.0003	0.003	MHz
g_x	2.86	0.07	0.07	kHz/G
g_y	3.05	0.11	0.11	kHz/G
g_z	11.56	0.03	0.1	kHz/G
α_M	-99.7	0.4	1	deg.
β_M	55.7	0.2	1	deg.
γ_M	-40	20	20	deg.
α_Q	-94	1	1	deg.
β_Q	58.1	0.4	1	deg.
γ_Q	-20.7	2.0	2	deg.
C_2 azimuth	87.8	0.1	1	deg.
C_2 elevation	-1.9	0.1	1	deg.

TABLE II. Results of fitting of the excited state.

Quantity	Value	Random uncertainty	Total uncertainty	Units
E	0.4228	0.0001	0.003	MHz
D	1.3575	0.0002	0.003	MHz
g_x	1.56	0.05	0.05	kHz/G
g_y	1.44	0.02	0.02	kHz/G
g_z	3.41	0.02	0.05	kHz/G
α_M	-178.2	0.7	1	deg.
β_M	59.6	0.6	1	deg.
γ_M	116	18	18	deg.
α_Q	90.1	0.7	1	deg.
β_Q	54	2	2	deg.
γ_Q	15.8	1.6	2	deg.
C_2 az.	86.9	0.2	1	deg.
C_2 elev.	2.8	0.4	1	deg.

pseudoquadrupole tensors for both the ground and excited state are aligned.

The authors recognize that working with such a low symmetry system increases the chance that the fit may be fortuitous. We are confident in our result because of the range of magnetic field directions used and the robust nature of simulated annealing. Values for some of the parameters were known independent of the fitting procedure (quadrupole parameters and position of the C_2 axis) and the fitted and *a priori* values agreed with each other within the respective uncertainties.

VI. CALCULATED OSCILLATOR STRENGTHS

Once the pseudoquadrupole and Zeeman tensors for both the ground and excited state are known it is possible to calculate the oscillator strengths and transition frequencies for each transition and for each magnetic field value. As an example of this we calculate the relative optical oscillator strengths for optical transitions between ground and excited state hyperfine manifolds. The nuclear projection does not change in an optical transition and thus the relative strength of a transition is given by the overlap of the nuclear states.

The Hamiltonian for both the ground and excited states in zero field was numerically diagonalized and the inner product between each pair of eigenvectors calculated. The results are shown in Table III. The z axis for the calculation was the major axis of the pseudo-quadrupole ellipsoids, which is the same for both the ground and excited states.

TABLE III. Overlap of the nuclear states between the ground and optically excited hyperfine manifold. Each column refers to a particular ground state level and each row refers to a particular excited state level. The states are labeled by the conventional notation $\pm n/2$ where $n=1,3,5$ although it should be noted that the eigenstates of the Hamiltonian are in general far from angular momentum eigenstates.

	$-5/2$	$-3/2$	$-1/2$	$+1/2$	$+3/2$	$+5/2$
$-5/2$	0.99	$+0.03$	$+0.09$	-0.00	-0.06	$+0.00$
$-3/2$	$+0.00$	-0.88	-0.00	-0.19	-0.43	$+0.08$
$-1/2$	$+0.07$	-0.09	$+0.98$	-0.02	$+0.18$	-0.00
$+1/2$	-0.00	-0.18	$+0.02$	$+0.98$	-0.09	-0.07
$+3/2$	$+0.08$	$+0.43$	$+0.19$	-0.00	-0.88	-0.00
$+5/2$	-0.00	-0.06	-0.00	-0.09	-0.03	-0.99

The states are labeled by the conventional notation $\pm n/2$ where $n=1,3,5$ although it should be noted that the eigenstates of the Hamiltonian are in general far from angular momentum eigenstates. To illustrate this the values of $\langle J_z \rangle$ are $\pm 2.49, \pm 0.85, \pm 0.39$ for the ground state hyperfine levels and $\pm 2.43, \pm 1.10, \pm 0.17$ for the excited state hyperfine levels.

In order to create EIT in such materials one needs to choose two ground state levels and one excited state level. These should be chosen to obtain a reasonable oscillator strength for each transition. The results of Table III suggest the "$\pm 1/2$" and "$\pm 3/2$" as ground states and either the "$\pm 1/2$" or "$\pm 3/2$" excited state should be used for efficient EIT in the case of zero magnetic field. This confirms the choice of the transitions used by Ham *et al.*[1]

VII. CONCLUSION

We have characterized the hyperfine manifolds for the ground and one optically excited state of praseodymium dopants in Y_2SiO_5. This enables the transition frequencies and oscillator strengths for any transition between or within the manifolds to be calculated for an arbitrary applied magnetic field. This allows the conditions for future EIT experiments in this material to be optimized.

*Electronic address: jevon.longdell@anu.edu.au

[1] B.S. Ham, P.R. Hemmer, and M.S. Shahriar, Opt. Commun. **144**, 227 (1997).
[2] K. Ichimura, Opt. Commun. **196**, 119 (2001).
[3] A.V. Turukhin, V.S. Sudarshanam, M.S. Shahriar, J.A. Musser, B.S. Ham, and P.R. Hem, Phys. Rev. Lett. **88**, 023602 (2002).
[4] R.W. Equall, Y. Sun, R.L. Cone, and R.M. Macfarlane, Phys. Rev. Lett. **72**, 2179 (1997).
[5] M.A. Teplov, Sov. Phys. JETP **26**, 872 (1968).
[6] J.M. Baker and B. Bleaney, Proc. R. Soc. London, Ser. A **245**, 156 (1958).
[7] J. Mlynek, N.C. Wong, R.G. DeVoe, E.S. Kintzer, and R.G. Brewer, Phys. Rev. Lett. **50**, 993 (1983).
[8] N.C. Wong, E.S. Kintzer, J. Mlynek, R.G. DeVoe, and R.G. Brewer, Phys. Rev. B **28**, 4993 (1983).
[9] H. Goldstein, *Classical Mechanics* (Addison-Wesley, Reading, MA, 1980).
[10] S. Kirkpatrick, C.D. Gelatt, and M.P. Vecchi, Science **220**, 671 (1983).